Nonlinear absorption and scattering properties of cadmium sulphide nanocrystals with its application as a potential optical limiter

N. Venkatram, R. Sai Santosh Kumar, and D. Narayana Rao

Citation: J. Appl. Phys. **100**, 074309 (2006); doi: 10.1063/1.2354417
View online: http://dx.doi.org/10.1063/1.2354417
View Table of Contents: http://jap.aip.org/resource/1/JAPIAU/v100/i7
Published by the American Institute of Physics.

Nonlinear absorption and scattering properties of cadmium sulphide nanocrystals with its application as a potential optical limiter

N. Venkatram, R. Sai Santosh Kumar, and D. Narayana Rao[a)]
School of Physics, University of Hyderabad, Hyderabad 500 046, India

(Received 8 May 2006; accepted 6 July 2006; published online 9 October 2006)

A systematic study of nonlinear absorption and scattering properties of 4.5 nm sized CdS nanocrystals dispersed in dimethylformamide with varying concentrations is reported in this paper. The study is undertaken by performing open aperture *Z*-scan measurements with 532 nm nanosecond and 790 nm femtosecond pulse excitations. A modified *Z*-scan experimental setup is used to collect both nonlinear absorption and nonlinear scattering at different forward angles simultaneously. Optical limiting studies of these nanocrystals show that nonlinear scattering (NLS) is comparable to the two-photon absorption (TPA). Both the TPA and NLS coefficients are estimated by theoretical fit of the observed open aperture *Z*-scan curves. The variation of NLS coefficients with concentration is discussed in detail, and we estimated the thermo-optic coefficient of CdS nanocrystals. The nonlinear refractive index and limiting threshold ($I_{1/2}$) of CdS nanocrystals at different concentrations (at 532 nm) are also estimated and reported. Further, we report our observation of the formation of diffraction fringes in the transmitted beam at high intensities.
 [DOI: 10.1063/1.2354417]

I. INTRODUCTION

In recent years, interest in the synthesis, characterization, and application of colloidal "quantum dot" semiconductor materials has grown markedly.[1] Nanocrystals of cadmium sulfide (CdS) are by far the most studied system among all the semiconducting nanocrystals.[2] The bulk CdS has a direct band gap of 2.4 eV at 300 K, and the typical Bohr exciton diameter of CdS is around 5.8 nm; consequently, CdS nanocrystals in the size range of 1–6 nm show sizable quantum confinement effects with remarkably different optical properties. The size dependent, unusual optical and electronic properties of these nanocrystals have been studied in detail using a wide variety of experimental and theoretical techniques.[3–5] The changes in the properties of nanocrystals are driven mainly by two factors, namely, the increase in the surface to volume ratio and drastic changes in the electronic structure of the material due to quantum mechanical effects with decreasing crystal size. Very often, it is an interplay of these two effects that is responsible for the changes in the properties.[6] For sizes as small as a few nanometers, the surface atoms, which can be neglected for a bulk solid material, play a major role in determining the electronic properties. The linear optical properties of semiconductor nanocrystals depend strongly on crystal size, for example, the blueshift of excitonic absorption and emission peaks with decreasing crystal size is a well-known observation. The unusual properties of the nanocrystals, in the quantum-confined regime, have led to numerous technological applications. Of late, owing to significant improvement in the synthetic methods, narrow size distribution of the crystallites is made possible.[7–9] CdS nanocrystals have been synthesized using a variety of methods employing polymers,[10] glasses,[11] zeolites,[12] reverse micelles,[13] and the method of arrested precipitation using suitable organic moieties.[7] In the past decade, there has been increasing interest in the luminescent and nonlinear optical properties of these nanometer-sized semiconductor crystals.[14] Large optical nonlinearities in CdS nanocrystals have been reported using different techniques.[15–19] These techniques include degenerate four-wave mixing and *Z*-scan techniques with nanosecond and picosecond laser pulses. *Z* scan, especially, is an effective technique to investigate nonlinear absorption and nonlinear refraction. Using the *Z*-scan technique we have previously described the nonlinear absorption and scattering properties of thioglycerol capped 4.5 nm sized CdS nanocrystals.[20] Strong two-photon absorption and nonlinear scattering are found to be responsible for good optical limiting characteristics in these nanocrystals. An ideal optical limiter, by definition, is a device that exhibits a linear transmittance below a threshold and clamps the output to a constant above it, thus providing safety to sensors and the eyes. A wide range of materials contributing to the optical limiting and nonlinear absorption has been investigated.[21,22] It is well known that optical limiting devices rely on one or more of the nonlinear optical mechanisms[14] such as excited state absorption, free-carrier absorption, two-photon absorption (TPA), thermal defocusing/scattering, photorefraction, nonlinear refraction, and induced scattering with enhancement in limiting performance by coupling two or more of such mechanisms.[23,24] Han *et al.*[25] observed strong nonlinear absorption in Ag_2S/CdS particles prepared by inverse microemulsion technique, but they observed poor optical limiting performance. In our earlier report[20] the CdS nanocrystals synthesized by a chemical method and monodispersed in dimethylformamide (DMF) were observed to have lower limiting threshold and a better optical limiting performance.

In this paper, we present detailed study of the effect of

[a)]Author to whom correspondence should be addressed; electronic mail: dnrsp@uohyd.ernet.in

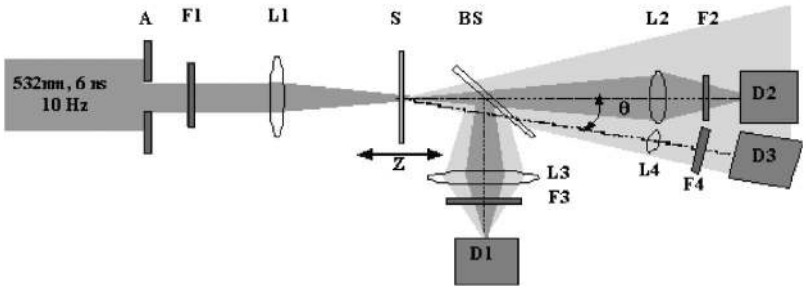

FIG. 1. Schematic of the *Z*-scan setup for recording the nonlinear absorption and scattering. A—aperture; S—sample; F1, F2, F3, and F4—Neutral density filters, D1, D2, and D3—detectors; BS—beam splitter; L1, L2, L3, and L4—lens.

concentration on the nonlinear optical properties of 4.5 nm sized thioglycerol capped CdS nanocrystals and estimate the parameters such as the two-photon absorption coefficient (β), the nonlinear scattering coefficient (α_s) of CdS nanocrystals at different concentrations (at 532 nm), thermally induced nonlinear refractive index change (Δn_{th}), and second order hyperpolarizability (γ). From the variation of α_s with concentration, we estimated the thermo-optic coefficient (dn/dT) of 4.5 nm size CdS nanocrystals. We report the limiting threshold as a function of the concentration of CdS nanoparticles. We also report the observation of the circular diffraction fringes in the transmitted beam.

II. EXPERIMENT

CdS nanocrystals with an average size of 4.5 nm are synthesized following the procedure suggested by Vossmeyer *et al.*[8] using thioglycerol as capping agent. The precursors used, 2.35 g (8.82 mmol) of cadmium acetate dihydrate, 0.473 g (6.24 mmol) of thiourea, and 0.95 ml (10.95 mmol) of thioglycerol added to 5 ml of DMF, are heated at 110 °C for 1 h under nitrogen atmosphere, followed by refluxing the mixture for 12–14 h. The solution is then condensed to about 1/10 of its original volume using a rotary evaporator. Following this, the yellowish thioglycerol capped CdS nanocrystals obtained are washed with acetone and ether.

Nonlinear absorption studies are carried out using the open aperture *Z*-scan technique.[26] In a typical *Z*-scan experimental setup, a laser beam with a transverse Gaussian profile is focused using a lens. The sample is then moved along the propagation direction of the focused beam. At the focal point, the sample experiences maximum pump intensity, which gradually decreases in either direction from the focus. A $f/24$ configuration is used for the present studies. A frequency doubled Nd:YAG (yttrium aluminum garnet) laser (Spectra-Physics, INDI 40, 532 nm, 6 ns, 10 Hz) is used as the excitation source. Apertures are introduced in the path for beam shaping and calibrated neutral density filters are used to vary the laser intensity. The thickness of the sample is chosen in such a way that it is smaller than the Rayleigh range of the focused beam calculated to be ~3 mm. The values of beam waist at focus are ~20–30 μm and the corresponding peak intensities are $\sim 10^8$–10^9 W cm^{-2}. A 50-50 beam splitter introduced immediately after the sample collects the transmitted light that includes scattered light. This reflected beam is focused onto detector 1 by using a large area lens. Detector 1, therefore, sees only the losses due to linear and nonlinear absorptions of the sample. The other half of the transmitted beam after the beam splitter is collected with a small area lens at far field to reduce the scattered light falling on detector 2. Hence, detector 2 accounts for the absorptive as well as scattering losses. Figure 1 shows the experimental setup for the *Z*-scan experiment. The sample cell and the beam splitter are mounted on a translation stage and detector 1 along with the collection lens L3 are positioned accordingly. The scattering at different forward scattering angles with beam propagation direction is collected using detector 3. The data are recorded by scanning the cell across the focus, and the transmitted beam was focused onto the photodiode (FND-100) with a lens. A boxcar averager (model SR250) is used for signal averaging, the output of which is given to a computer with an analog-to-digital converter (ADC) card. The cell is translated along the beam propagation direction using a computer controlled stepper motor and the data are collected at steps of 0.375 mm.

III. RESULTS AND DISCUSSION

The adopted synthesis procedure resulted in ~30% yield of about 1.02 g of yellowish CdS nanocrystals. For our studies, these nanocrystals were dispersed in DMF by forming a clear yellowish colloidal solution. The UV/visible absorption spectrum of the nanocrystals was recorded at room temperature with a spectrophotometer (Shimatzu 3101PC). We find, as shown in Fig. 2, a sharp absorption peak at 415 nm, which

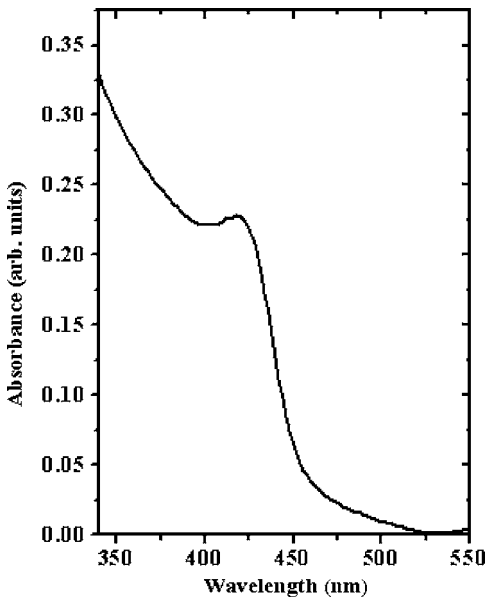

FIG. 2. UV-Vis absorption spectra of CdS nanocrystals.

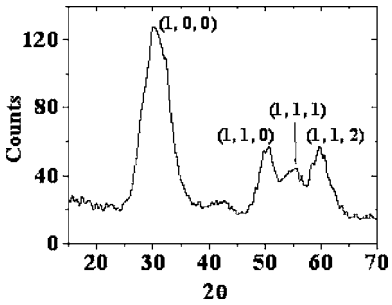

FIG. 3. XRD spectra of CdS nanocrystals.

clearly indicates the monodispersity of CdS nanocrystals. The absorption peak is blueshifted from that of the bulk CdS, which is around 532 nm.[27]

The size measurements and surface morphology of the CdS nanocrystals are carried out by powder x-ray diffraction spectrometer (INEL x-ray diffraction spectrometer with Co target) and transmission electron microscope (TEM) studies. From the x-ray diffraction (XRD) spectra of CdS, as shown in Fig. 3, it is very evident that the nanocrystals formed are crystalline in nature. From the spectra the (h,k,l) planes and average grain size are determined. The crystal size (D) is calculated using the *Scherer formula*,[28] $D=(0.9\lambda)/(B\cos\theta)$, where λ is the wavelength of the x radiation, B is the full width at half maximum (FWHM) of the XRD peak, and θ is the half of the Bragg angle at maximum peak height. Though one could get a rough estimate of the average grain size using the XRD data, a better estimate of the crystal size is obtained by TEM studies. The TEM pictures are taken on copper grid with JEOL (100CX) unit and the high-resolution TEM (HRTEM) pictures are taken on carbon coated copper grids with JEOL (JEM-2010) system.

The TEM pictures of the CdS nanocrystals are as shown in Fig. 4(a). The monodispersity of nanocrystals in DMF is very evident from the figure indicating that the nanocrystals are well separated from each other. This is expected because of the presence of a thiol group, which is known to be a surface passivating ligand. Using the HRTEM images recorded for the CdS nanocrystals, we observe that the CdS nanocrystals have hexagonal crystal structures. Figure 4(b) shows the crystalline planes inside the thioglycerol capped CdS nanocrystals. The observed interplanar distance d is 0.338 nm. The inset shows the diffraction pattern of CdS nanocrystals in which each circle corresponds to a single plane of the crystal. The (h,k,l) values of the planes calculated, taking into account the hexagonal crystal structure of the CdS, are (1,0,0), (1,1,0), (1,1,1), and (1,1,2) and agree with the XRD data.

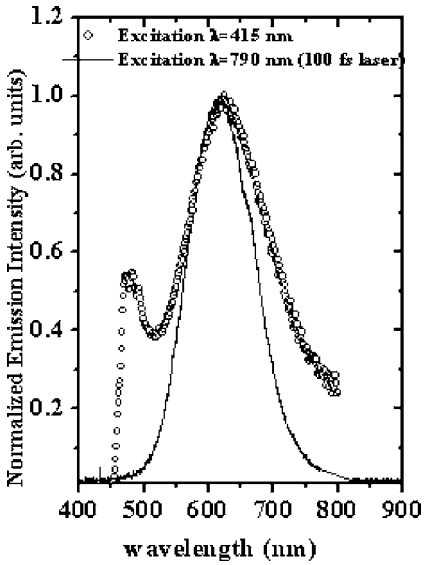

FIG. 5. Fluorescence and upconverted fluorescence spectra of the CdS nanocrystals.

The emission property of these nanocrystals is studied by recording the fluorescence spectrum (Jobin Yvon Horiba FluoroMax-3) with excitation at 415 nm. Figure 5 shows the emission peaks, a broad peak at 617 nm and a sharp peak at 482 nm. The 482 nm emission is the band edge emission peak, which is close to the excitation wavelength, while the broad emission peaking at 617 nm is contributed by the presence of trap states.[29] The deep trap states are mostly due to the sulfur vacancies. Emission from CdSe nanoparticles has been reported[30] to be due to trap states. The band edge emission decay is observed to be faster than the trap state emission decay. The black solid line in the figure shows the two photon excited fluorescence spectra excited with 790 nm, ~100 fs pulses (Spectra-Physics, Maitai-Spitfire) that has the emission maxima at 615 nm. Here CdS nanocrystals absorb two photons of 790 nm to go to the conduction band and emit a single photon of wavelength 615 nm.

The open aperture Z-scan data recorded by placing the detectors at two positions as explained in the experimental section is shown in Fig. 6. The CdS nanocrystals show strong reverse saturable absorption (RSA) behavior at all intensities. Detector 1 gives the "whole transmitted light" due to the

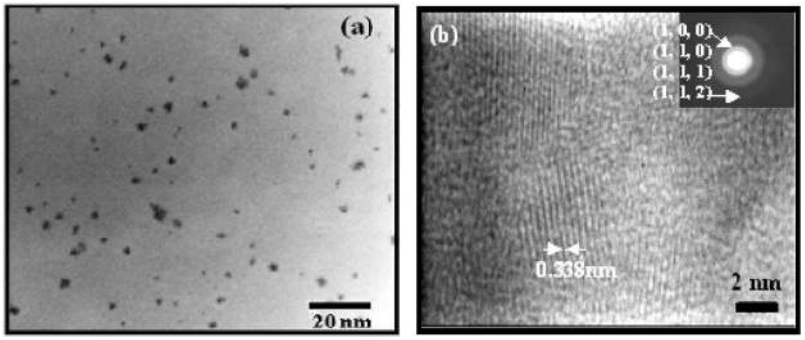

FIG. 4. (a) TEM picture of CdS nanocrystals. (b) HR-TEM picture of CdS nanocrystals showing crystalline structure and diffraction pattern (inside picture).

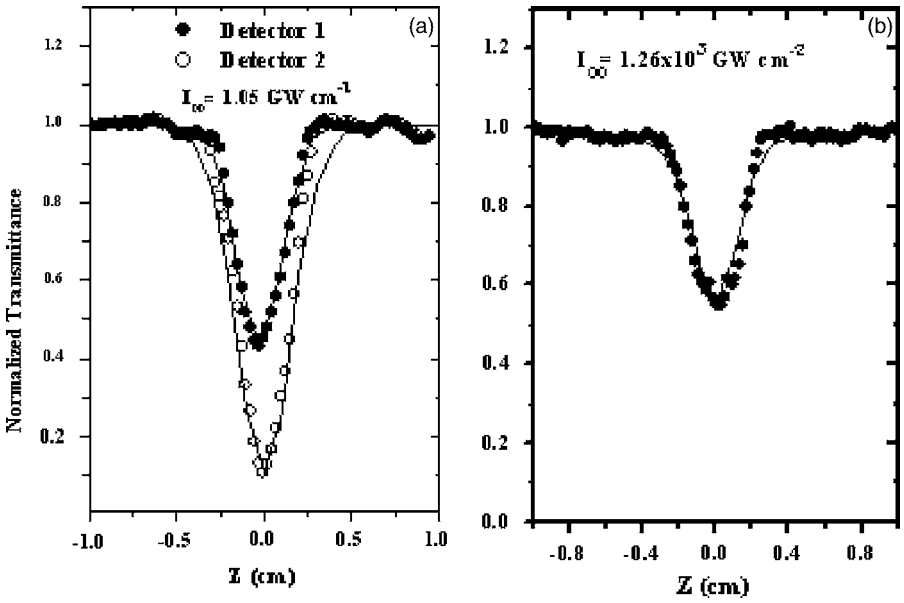

FIG. 6. (a) Open aperture *Z*-scan curves of the CdS nanocrystals (concentration=10.4×10^{-2} M/L) collected with two detectors; detector 1 gives the transmitted light and scattering, and detector 2 gives the transmitted light without scattering with 6 ns laser pulses. (b) Open aperture *Z*-scan curve of the CdS nanoparticles with 100 fs laser pulses, and the solid line is the curve obtained by theoretical fitting.

nonlinear two-photon absorption alone. Detector 2 kept at the far field gives the transmitted beam minus the scattered beam due to both two-photon absorption and the nonlinear scattering losses with 6 ns pulses. At peak intensities >100 MW cm^{-2} we see nonlinear scattering along with strong TPA. This can be seen as an enhanced depletion in the transmitted beam collected with detector 2, which is reflected in the *Z*-scan curve shown in Fig. 6(a). The transmittance goes to as low as 0.1 when the loss due to the nonlinear scattering is taken into account. However, *Z*-scan data taken with 790 nm, 100 fs pulses collected with detector 2 [shown in Fig. 6(b)] show negligible scattering. As the CdS nanoparticles show strong TPA, the scattering observed with the nanosecond pulses is attributed to the local heating of CdS nanoparticles. The nonlinear scattering behavior of the CdS nanocrystals as a function of the input intensity (*Z* position) is as shown in Fig. 7(a), in which the curves shown are of those obtained for three different forward scattering angles with beam propagation direction using detector 3. It is observed that the nonlinear scattering is conical in nature with the intensity decreasing as we go away form the center. Figure 7(b) shows the snapshot of the transmitted beam, which explains the above-mentioned observation.

To account for the losses as seen in detector 2, we have introduced the nonlinear scattering losses α_s as derived by Joudrier *et al.*[31] From the absorption spectra of CdS nanocrystals (Fig. 2), we clearly see that the linear absorption coefficient is very small at the excitation wavelength of 532 nm. Thus in our analysis we have neglected the contribution of the linear absorption cross section. Since CdS is a direct band gap semiconductor, a two-level model corresponding to valence and conduction bands is used to explain the observed results. By using this model, we first estimated the two-photon absorption coefficient β using α_s as zero by fitting the *Z*-scan curve, which we got from detector 1. We then used this value to estimate the nonlinear scattering coefficient α_s from the curve obtained from detector 2. The treatment of this theoretical modeling is as reported in our earlier report.[20] The differential Eqs. (1) and (2) are taken as the two rate equations for the valence band and the conduction band populations and the intensity transmitted through the sample is given by Eq. (3).

$$\frac{dN_0}{dt} = -\frac{\beta I^2}{2\hbar\omega} + \frac{N_1}{\tau_1}, \tag{1}$$

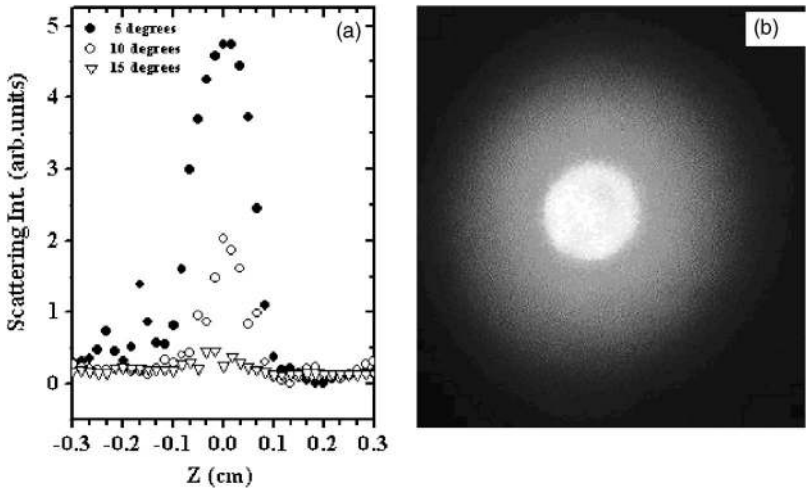

FIG. 7. (a). Scattering of CdS nanocrystals at three different forward angles with intensity (*Z*-position). (b) Snapshot of the transmitted beam showing the distribution of the scattering in transmitted light through the CdS nanocrystals.

$$\frac{dN_1}{dt} = \frac{\beta I^2}{2\hbar\omega} - \frac{N_1}{\tau_1}, \tag{2}$$

$$\frac{dI}{dz} = -\alpha_s I - \beta I^2, \tag{3}$$

where

$$\alpha_s = g_s(\Delta\tilde{n})^2,$$

$$\Delta n = \Delta n_l + \Delta n_{\mathrm{nl}}.$$

Here N_0 and N_1 are populations of valence band and conduction band, respectively, α_s is the effective scattering coefficient, β is the two-photon absorption coefficient, g_s is a parameter independent of intensities but depends on the size, shape, and concentration of crystals and wavelength of light, $\Delta\tilde{n}$ is the difference in the effective refractive indices of both linear and nonlinear components, Δn_l is the difference in the linear refractive indices of CdS and DMF, Δn_{nl} is the difference in nonlinear refractive indices of CdS and DMF, which is a function of intensity, and τ_l is the lifetime of the excited state and is taken as 114 ps.[17] The differential equations are solved numerically using the Runge-Kutta fourth order method. The equations are first decoupled and then integrated over time, length, and along the radial direction. Assuming the input beam to be Gaussian, the limits of integration for r, t, and z are varied from 0 to ∞, from $-\infty$ to ∞, and from 0 to L (length of the sample), respectively. Typical number of slices used for r, t, and z are 60, 30, and 5, respectively. $g_s\Delta n_l$, $g_s\Delta n_{\mathrm{nl}}$, β, and α_s are then estimated through least square fitting of the experimental data. From the calculated value for $g_s\Delta n_l$, we have determined the scattering constant g_s. The two-photon absorption cross section (σ_{TPA}) is then calculated from[32]

$$\sigma_{\mathrm{TPA}} = \frac{h\nu}{N}\beta,$$

$$N = N_A D, \tag{4}$$

where N is the number of molecules per unit volume, D is the molar concentration of CdS, N_A is the Avogadro constant, h is Planck's constant, and ν is the frequency of laser beam used. Five different concentrations of CdS nanocrystals, dispersed in DMF, were used for the concentration dependent studies. The open aperture Z-scan studies and the theoretical data fit were carried out much in the similar fashion at several intensities as described above. The values of the different parameters of our interest with varied concentrations were estimated and presented in Table I. As expected, it is observed that the two-photon absorption coefficient (β) increases linearly with concentration as shown in Fig. 8. The nonzero intercept on the y axis at 9.3×10^{-9} cm W^{-1} is due to the TPA coefficient of the solvent. This has been confirmed by recording the Z-scan curves of the pure solvent at higher intensities (as the TPA is very weak in the pure solvent) and estimating the β value separately. With increase in concentration, the number of crystals per unit area of interaction with the laser beam increases, as a result of which, we see an increase in the values of β. We calculated two-photon absorption cross section (σ_{TPA}) of the CdS nanocrystals from Eq. (4) by taking into account the β value estimated for each concentration. The σ_{TPA}, being a material property, is independent of concentration and is determined to be 1.07×10^{-42} cm^4 s photon^{-1} particle^{-1} (1.12×10^{-46} cm^4 s photon^{-1} molecule^{-1}, when calculated using the density of CdS as 4.82 g cm^{-3} and for a particle size of 4.5 nm diameter).

TABLE I. Two-photon absorption coefficient (β), nonlinear scattering coefficient (α_s), scattering parameter (g_s), thermal nonlinear refractive index [$\Delta n_{\mathrm{th(CdS)}}$], and limiting threshold ($I_{1/2}$) of CdS nanocrystals at different concentrations (at 532 nm wavelength).

Concentration of CdS in DMF (10^{-2} M/L)	β (10^{-8} cm W^{-1})	α_s (cm^{-1})	$\Delta n_{\mathrm{th(CdS)}}$ (10^{-6} cm^2 W^{-1})	Limiting threshold $I_{1/2}$ (J cm^{-2})
0.865	1.29	114.7	−20.7	1.4
1.66	1.44	133.4	−15.0	1.29
1.87	1.49	172.3	−11.7	1.25
4.50	1.98	186.5	−5.1	0.96
8.30	2.61	167.2	−2.66	0.6
10.40	3.15	146.2	−2.01	0.43

Degenerate four-wave mixing (DFWM) was carried out with 6 ns, 532 nm Nd:YAG as the pump. In the DFWM setup, we used counterpropagating geometry, in which three beams of equal intensity are derived from the same beam. The probe makes an angle of ~10° with one of the pumps, while the pumps are counterpropagating to each other. All three beams are focused into the sample kept in a 1 mm cuvette and the phase conjugate (PC) signal was collected with a photodetector. The PC signal plot as a function of the intensity in Fig. 9 having a slope of ~5, whereas the slope of the CS_2 is ~3, indicates that the dominant process is strong TPA.

As stated earlier, $\Delta\tilde{n}$ is the difference in the effective refractive indices of both linear and nonlinear components, Δn_l is the difference in the linear refractive indices of CdS

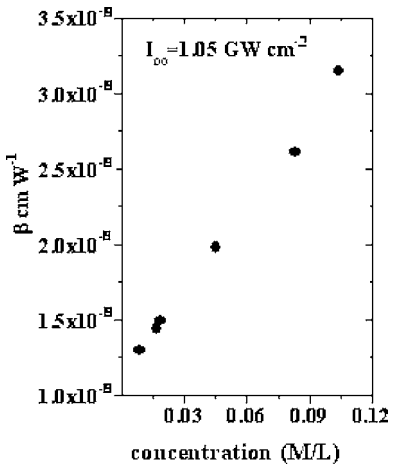

FIG. 8. Change in two-photon absorption coefficient (β) with respect to concentration of CdS nanocrystals. β, as estimated from the Z-scan data recorded with a nanosecond laser of pure DMF solvent is 9.3×10^{-9} cm W^{-1}.

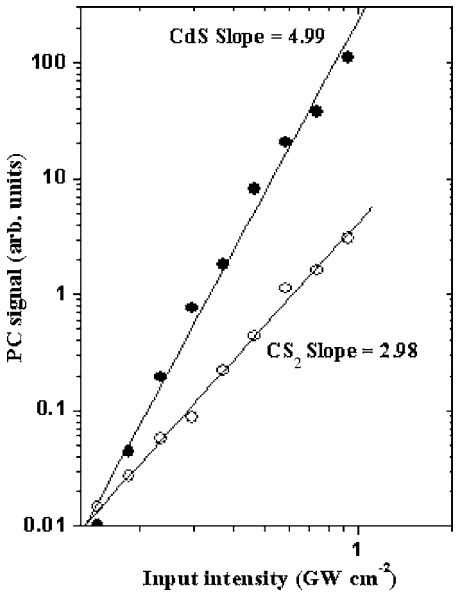

FIG. 9. Log-log plot of the phase conjugate signal as a function of the intensity, CdS curve having a slope of ~5 and CS_2 curve having a slope of ~3.

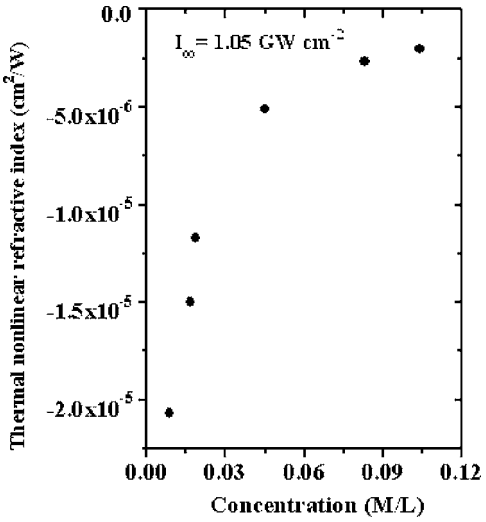

FIG. 10. Change in thermal nonlinear refractive index (Δn_{th}) with respect to concentration of CdS nanocrystals.

and DMF, wherein linear refractive indices of the CdS and DMF are taken as 2.4 and 1.42, respectively, and Δn_{nl} is the difference in nonlinear refractive indices of CdS and DMF. The intensity dependent study revealed that the nonlinear scattering starts showing up at intensities ~100 MW cm^{-2} and increases with increase in the input intensity, thus becoming almost comparable to the contribution of TPA losses at higher intensities. In order to estimate the contribution of real and imaginary parts towards the n_{2eff},[33,34] we carried out the DFWM experiment with a 100 fs laser at 790 nm. Comparing the signals of CdS and CS_2 in DFWM experiments using the boxcar geometry with the femtosecond laser at 790 nm, we estimate the value of $\chi^{(3)}$ of CdS as 3.3×10^{-12} esu at a concentration of 0.1 M/L. The second hyperpolarizability γ of CdS nanoparticles is estimated as 1.19×10^{-29} esu particle^{-1} (1.24×10^{-33} esu molecule^{-1}, when calculated using the density of CdS as 4.82 g cm^{-3} and a particle size of 4.5 nm diameter). As this value is measured with a femtosecond laser, we have taken it as due to the real part of $\chi^{(3)}$. As it is several orders of magnitude smaller than the signals measured with the nanosecond laser, we have taken the signals obtained in DFWM with a nanosecond laser (532 nm) as mainly due to TPA and to be thermal in nature.

The observed scattering is attributed to the difference in the refractive indices of CdS and DMF and comes from both the linear and nonlinear components. As CdS shows strong two-photon absorption, the nonlinear refractive index has a strong thermal contribution to the measured n_{2eff} value of CdS and the thermal contribution increases at higher intensities. Since the nonlinearity of DMF is very small compared to that of CdS, we neglect the contribution of the nonlinear refractive index of DMF and simply consider Δn_{nl} to be just n_{2eff} (of CdS). The variation of n_{2eff} with concentration is as shown in Fig. 10. The Δn_{th} between the CdS and DMF is the same as n_{2eff} of CdS, which in our case is due to thermalization of the CdS nanoparticles.[35] Resonant excitation with nanosecond and longer pulses can result in thermally induced transient refractive index changes given by,[26]

$$\Delta n_{th(CdS)} = n_{2\,eff} = \frac{dn}{dt}\frac{F_0\alpha}{2\rho_0 C_p}, \tag{5}$$

where dn/dt is the thermo-optic coefficient, F_0 is the light fluence, C_p is the specific heat of CdS (330 J kg^{-1} K^{-1}),[36] ρ_0 the medium density, $\frac{1}{2}$ comes from the fluence averaging, and α is the multiphoton absorption coefficient of the CdS nanocrystals. α for CdS is calculated by[37]

$$\alpha = nN\sigma[I(r,t)]^{n-1}, \tag{6}$$

where n is the order of absorption process ($n=2$ for TPA). Using the values of σ, $I(r,t)$, and N, the two-photon absorption cross section per molecule (cm^4 s molecule^{-1} photon^{-1}), the incident photon flux (photons cm^{-2} s^{-1}), and number of molecules per cm^3, respectively, α is estimated as 1.10×10^{-2} molecule^{-1} cm^{-1}.

The variation of nonlinear scattering coefficient (α_s) with concentration resembles an inverted parabola having a maximum for α_s at around 4.5×10^{-2} M/L as shown in Fig. 11. In order to explain the observed change of α_s, we fitted the experimental data with the following relation, which is derived from the definition of α_s stated earlier:

$$\alpha_s = g_s(\Delta n_l + n_{2\,eff} I)^2, \tag{7}$$

where I is the intensity of the exciting beam. It is observed that g_s has cubic dependence on concentration. Figure 11 shows the plot of α_s as a function of the concentration of CdS nanocrystals in DMF at two different intensities. The solid points are the experimental data and the continuous line is the calculated values of α_s obtained from Eq. (7). From the fit we estimated the thermo-optic coefficient dn/dT of CdS nanocrystals to be -1.58×10^{-6} K^{-1}. In Fig. 11 we see that α_s increases with concentration up to 4.5×10^{-2} M/L and decreases with further increase in concentration. This behavior can be rationalized by considering the extent of nonuniform heating of the sample at the focus induced due to the two-photon absorption of CdS nanocrystals present in the

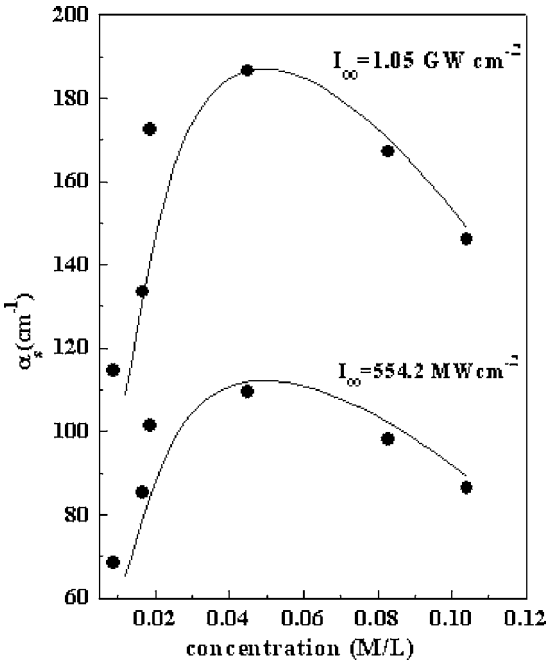

FIG. 11. Change in effective scattering coefficient (α_s) with respect to concentration of CdS nanocrystals at two different intensities. The solid line is the curve obtained by fitting Eq. (7).

focal volume. This nonuniform heating corresponds to the change in the effective refractive index difference between the two components of the medium. At lower concentration the nanocrystals are far apart from each other resulting in less nonuniform heating. As the concentration of CdS increases, there is corresponding increase in the nonuniform heating until it reaches a maximum, which corresponds to the concentration of 4.5×10^{-2} M/L. However, with further increase in the concentration the CdS nanocrystals move closer to each other, which leads to more uniform heating of the CdS nanocrystals, and the solvent reduces the Δn_{th} contribution in the scattering.

Because of the strong nonlinear absorption and nonlinear scattering properties, these nanocrystals are suitable for the optical limiting (OL) application. The observed scattering behavior is quite interesting in the sense that no scattering was observed below 100 MW cm^{-2} and at higher intensities the scattering losses help achieve better limiting thresholds. Thus, CdS nanocrystals serve as good scatterer at high intensities, without getting damaged due to nonlinear absorption alone. Figure 12 shows the optical limiting curves for the CdS nanocrystals for a concentration of 10.4×10^{-2} M/L in DMF. The solid line in the Fig. 12 represents a theoretical fit using Eq. (3). Clearly it can be seen that at higher intensities the losses due to nonlinear scattering is significantly large, henceforth enhancing the optical limiting by reducing the limiting threshold. The dependence of optical limiting threshold on concentration is shown in Fig. 13. It shows that limiting threshold decreases with increase in concentration of CdS nanocrystals. The last column of Table I shows the variation in limiting threshold with respect to concentration.

An interesting observation, which we made while carrying out the *Z*-scan experiments with the CdS nanocrystals, is the formation of circular optical fringes in the transverse

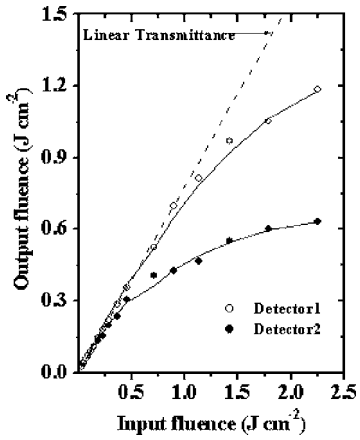

FIG. 12. Transmitted light and scattering (detector 1) and transmitted light without scattering (detector 2) of CdS nanocrystals (concentration=10.4 $\times10^{-2}$ M/L) with respect to input fluence. Dashed line represents linear transmittance of 0.76 at 532 nm and the solid line is the curve obtained by integrating Eq. (3).

plane to the beam propagation direction at a far field. This is observed only at high intensities ($I_{00}>1.0$ GW/cm^2). A snapshot of this observation is shown in Fig. 14. Recently several reports[38] have shown the formation of optical fringes when an intense laser beam passes through nanocrystallites as the refractive index of the material can be altered by the intensity of the laser beam as mentioned in this report. This change in the refractive index in the sample interacting with the laser beam acts similarly to that of a circular aperture with the size of the beam diameter in the sample, which in turn results in a diffraction pattern as seen in Fig. 14. More detailed study on this aspect is in progress and would be reported later.

We also synthesized CdS nanocrystals using glycerol as capping agent. However, the disadvantage of using glycerol as a capping agent is that the nanocrystals formed get agglomerated into bigger clusters of ~100 nm. In fact, these nanocrystals showed similar behavior in terms of nonlinear absorption and nonlinear refraction with good optical limiting properties.

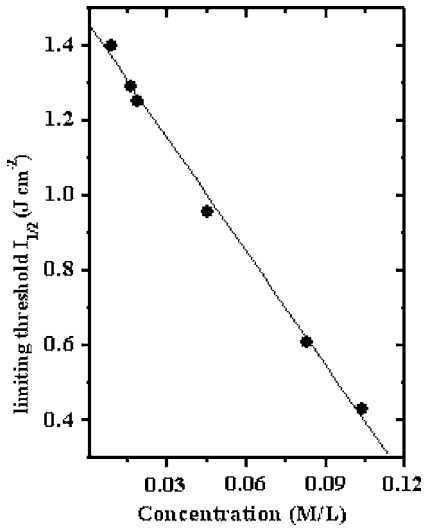

FIG. 13. Optical limiting threshold $I_{1/2}$ of CdS nanocrystals with respect to concentration, collected with detector 2.

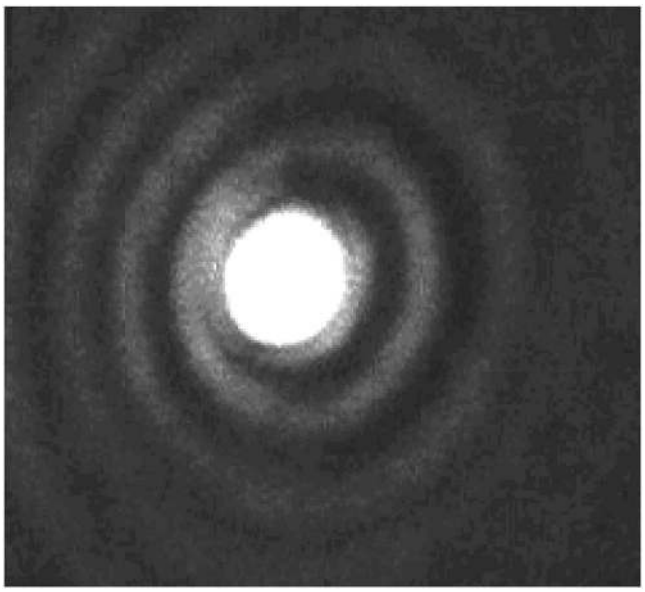

FIG. 14. Snapshot of circular optical fringes formed in the transverse plane to the beam propagation direction at high intensity.

IV. CONCLUSION

Nonlinear optical absorption and optical limiting behavior of thioglycerol capped CdS nanocrystals monodispersed in DMF were studied systematically along with their dependence on change in concentration of CdS nanocrystals in DMF. Enhanced RSA was observed in the *Z*-scan data showing an added component of losses due to nonlinear scattering along with the TPA. The losses due to nonlinear scattering were significant at high intensities. The obtained data were theoretically fitted with the help of a two-level model from which the two photon absorption coefficient (β), two-photon absorption cross section (σ_{TPA}), and nonlinear scattering coefficient (α_s) were calculated. The variation of α_s was discussed in detail by taking into account the refractive index variation due to $n_{2\mathrm{eff}}$ or $\Delta n_{\mathrm{th(CdS)}}$, which resulted in the estimation of the thermo-optic coefficient (dn/dT) for the 4.5 nm sized CdS nanocrystals. The optical limiting studies with change in concentration showed that the limiting threshold decreases linearly with increase in concentration. Efforts are underway to optimize the TPA coefficient by suitably tailoring CdS nanocrystals to achieve higher and better optical limiting performance. Apart from this we report the self-diffraction of CdS nanocrystals resulting in the formation of a fringe pattern in the transverse plane along the direction of propagation of the beam.

ACKNOWLEDGMENTS

Financial support from the Department of Science and Technology (DST—ITPAR), Government of India, is thankfully acknowledged. The authors thank Dr. Shashi Singh (CCMB, Hyderabad) and Dr. P. V. Satyam (IoP, Bhubaneswar) for the help with the TEM recording. Part of this work was supported by collaborative research scheme No. CRS/100/UH/P/DNR/8543 of UGC-DAE CSR-Kolkata Center. One of the authors (R.S.S.K.) acknowledges financial support of the Council of Scientific and Industrial Research (India).

[1] A. P. Alivisatos, J. Phys. Chem. **100**, 13226 (1996).
[2] H. Weller, Angew. Chem., Int. Ed. Engl. **32**, 41 (1993).
[3] L. E. Brus, J. Chem. Phys. **79**, 5566 (1983).
[4] M. V. Rama Krishna and R. A. Friesner, Phys. Rev. Lett. **67**, 629 (1991).
[5] P. E. Lippens and M. Lannoo, Phys. Rev. B **39**, 10935 (1989).
[6] S. A. Majetich and A. C. Karter, J. Phys. Chem. **97**, 8727 (1993).
[7] N. Herron, Y. Wang, and H. Eckert, J. Am. Chem. Soc. **112**, 1322 (1990).
[8] T. Vossmeyer, L. Katsikas, M. Giersig, I. G. Popovic, K. Diesner, A. Chemseddine, A. Eychmuller, and H. Weller, J. Phys. Chem. **98**, 7665 (1994).
[9] C. B. Murray, D. J. Norris, and M. G. Bawendi, J. Am. Chem. Soc. **115**, 8706 (1993).
[10] M. E. Wozniak and A. Sen, Chem. Mater. **4**, 753 (1992).
[11] T. M. Hayes, L. B. Lurio, and P. D. Persans, J. Phys.: Condens. Matter **13**, 425 (2001).
[12] Y. Wang and N. Herron, J. Phys. Chem. **91**, 257 (1987).
[13] C. Petit, P. Lixon, and M. P. Pileni, J. Phys. Chem. **94**, 1598 (1990).
[14] E. W. Van Stryland, H. Vanherzeele, M. A. Woodall, M. J. Soileau, A. L. Smirl, S. Guha, and T. F. Boggess, Opt. Eng. (Bellingham) **24**, 613 (1985).
[15] Y. Wang, A. Suna, J. McHugh, E. F. Hilinski, P. A. Lucas, and R. D. Johnson, J. Chem. Phys. **92**, 6927 (1990).
[16] R. A. Ganeev, A. I. Ryasnyansky, R. I. Tugushev, and T. Usmanov, J. Opt. A, Pure Appl. Opt. **5**, 409 (2003).
[17] J. He, W. Ji, G. H. Ma, S. H. Tang, H. I. Elim, W. X. Sun, Z. H. Zhang, and W. S. Chin, J. Appl. Phys. **95**, 6381 (2004).
[18] R. E. Schwerzel, K. B. Spahr, J. P. Kurmer, V. E. Wood, and J. A. Jenkins, J. Phys. Chem. A **102**, 5622 (1998).
[19] H. Du, G. Q. Xu, W. S. Chin, L. Huang, and W. Ji, Chem. Mater. **14**, 4473 (2002).
[20] N. Venkatram, M. A. Akundi, and D. Narayana Rao, Opt. Express **13**, 867 (2005).
[21] Y.-P. Sun and J. E. Riggs, Int. Rev. Phys. Chem. **18**, 43 (1999).
[22] L. W. Tutt and T. F. Boggess, Prog. Quantum Electron. **17**, 299 (1993).
[23] M. P. Joshi, J. Swiatkiewicz, F. Xu, P. N. Prasad, B. A. Reinhardt, and R. Kannan, Opt. Lett. **23**, 1742 (1998).
[24] F. E. Hernandez, S. Yang, E. W. Van Stryland, and D. J. Hagan, Opt. Lett. **25**, 1180 (2000).
[25] M. Y. Han, W. Huang, C. H. Chew, L. M. Gan, X. J. Zhang, and W. Ji, J. Phys. Chem. B **102**, 1884 (1998).
[26] M. Sheik-Bahae, A. A. Said, T. Wei, D. J. Hagan, and E. W. Van Stryland, IEEE J. Quantum Electron. **26**, 760 (1990).
[27] G. F. Bohren and D. R. Huffman, *Absorption and Scattering of Light by Small Particles* (Wiley, New York, 1983), p. 159.
[28] B. D. Cullity, *Elements of X-ray Diffraction* (Addison Wesley, New York, 1977).
[29] F. Wu, J. Z. Zhang, R. Kho, and R. K. Mehra, Chem. Phys. Lett. **330**, 237 (2000).
[30] M. Kuno, J. K. Lee, B. O. Dabbousi, F. V. Mikulec, and M. G. Bawendi, J. Chem. Phys. **106**, 9869 (1997).
[31] V. Joudrier, P. Bourdon, F. Hache, and C. Flytzanis, Appl. Phys. B: Lasers Opt. **67**, 627 (1998).
[32] Robert W. Boyd, *Nonlinear Optics*, 2nd ed. (Academic, New York, 2003).
[33] E. J. Canto-Said, D. J. Hagan, J. Young, and E. W. Van Stryland, IEEE J. Quantum Electron. **27**, 2274 (1990).
[34] M. Zhao, Y. Cui, M. Samoc, and P. N. Prasad, J. Phys. Chem. **95**, 3991 (1991).
[35] P. A. Fleitz, R. L. Sutherland, L. V. Natarajan, T. Pottenger, and N. C. Fernelius, Opt. Lett. **17**, 716 (1992).
[36] David R. Lide, *Handbook of Chemistry and Physics*, 86th ed. (CRS, Boca Raton, FL, 2005).
[37] A. J. Twarowski and D. S. Kliger, Chem. Phys. **20**, 253 (1977).
[38] H. S. Mavi, S. Prusty, A. K. Shukla, and S. C. Abbi, Opt. Commun. **226**, 405 (2003).